Journal of Magnetism and Magnetic Materials 326 (2013) 151–156

Contents lists available at SciVerse ScienceDirect

Journal of Magnetism and Magnetic Materials

journal homepage: www.elsevier.com/locate/jmmm

Electron paramagnetic resonance study of $(La_{0.33}Sm_{0.67})_{0.67}Sr_{0.33-x}Ba_xMnO_3$ ($x<0.1$): Griffiths phase

S.I. Andronenko [a], A.A. Rodionov [a], A.V. Fedorova [b], S.K. Misra [c,*]

[a] Kazan Federal University, 430008 Kazan, Russia
[b] St. Petersburg State University, 198054, St. Petersburg, Russia
[c] Physics Department, Concordia University, Montreal, Canada, H3G 1M8

ARTICLE INFO

Article history:
Received 18 June 2012
Received in revised form
13 August 2012
Available online 7 September 2012

Keywords:
Doped manganites
Electron paramagnetic resonance
Phase separation
Variable range hopping

ABSTRACT

Manganite compounds $(La_{0.33}Sm_{0.67})_{0.67}Sr_{0.33-x}Ba_xMnO_3$ with light Ba doping ($x=0.01$–0.09) have been investigated by electron paramagnetic resonance over the temperature range 110–450 K. It was found that the EPR linewidth behavior changed drastically in samples with these low Ba concentrations. For all the samples there was observed coexistence of paramagnetic and ferromagnetic phases below the phase-transition (Curie) temperature. EPR signals characteristic of a Griffiths phase were observed in the samples with $x=0.03$, 0.06, and 0.09. The temperature dependence of EPR linewidth in the paramagnetic phase was analyzed on the basis of the variable-range-hopping model, which explained the observed data.

1. Introduction

As reported previously [1–4], the magnetic properties and conductivity behavior of the manganite sample $(La_{0.33}Sm_{0.67})_{0.67}Sr_{0.33-x}Ba_xMnO_3$, with $x=0.0$, containing no Ba^{2+} ions, characterized by the phase-transition temperature $T_C=205$ K, are significantly different from those of the samples containing rather large amount of Ba ions, with $x=0.13$, 0.23, and 0.33, characterized by $T_C=127$ K, 112 K, and 96 K, respectively [1]. This indicates that T_C decreases sharply from 205 to 127 K for a rather small Ba doping of $x=0.13$, and then only to 96 K for Ba doping with the largest possible amount of $x=0.33$. In addition, the resistivity changed from $10^{-1}\,\Omega$ cm for $(La_{0.33}Sm_{0.67})_{0.67}Sr_{0.33}MnO_3$ at 100 K to about $10^3\,\Omega$ cm for all other samples ($x=0.13$, 0.23, 0.33) [1]. Thus, significant differences in magnetic and charge-transfer properties were observed in samples with Ba doping of $(La_{0.33}Sm_{0.67})_{0.67}Sr_{0.33-x}Ba_xMnO_3$. Therefore, investigation of behavior of such samples with light doping of Ba ions ($x<0.10$) is of special interest to develop further insight into the interactions among the various paramagnetic ions in these samples.

This paper reports an investigation of four manganite samples, $(La_{0.33}Sm_{0.67})_{0.67}Sr_{0.33-x}Ba_xMnO_3$, $x=0.01$, 0.03, 0.06, and 0.09, by X-band (~9.45 GHz) electron paramagnetic resonance (EPR) in the temperature range 110–450 K. In particular, the effects of substitution of the Sr^{2+} ion, with the ionic radius of 1.12 Å by the Ba^{2+} ion with the larger ionic radius of 1.34 Å, on the EPR spectra are investigated here. This substitution affects the structure of these compounds leading to a deviation from the structure of stoichiometric $LaMnO_3$, which is orthorhombic with space group Pnma ($T_N=140$ K) [5]. The degree of deviation depends on the ionic radius of the substituting divalent cation, leading to the rhombohedral structure with space group $R\bar{3}c$ for both $La_{0.67}Ba_{0.33}MnO_3$ ($T_C=343$ K) [6,7] and $La_{0.67}Sr_{0.33}MnO_3$ ($T_C=376$ K) [8,9].

2. Effect of ionic substitution in manganites

The amount of substituting ions governs the fractional contents of the Mn^{3+}($3d^4$, $L=2$) and Mn^{4+} ($3d^3$, $L=3$) ions present in the stoichiometric samples with the common formula $La_{0.67}B_{0.33}(Mn^{3+})_{0.67}(Mn^{4+})_{0.33}O_3$. The change in the average size of the cations at the B site of these perovskites causes large changes in their transport and magnetic properties due to modification of the Mn–O–Mn bond angles and Mn–O distances, thereby influencing the e_g electron hopping between the Mn^{3+} and Mn^{4+} states. In turn, such distortion of the bond angles and distances gives rise to competing superexchange and double-exchange interactions, causing electronic phase separation. Furthermore, increasing the Ba content in mixed Sr–Ba manganite leads to increasing disorder in the system, associated with an increasing spin-glass like behavior in these samples. Since diamagnetic La ions are partly substituted by the paramagnetic Kramers Sm^{3+} ions ($J=5/2$, $L=5$, $\mu_{eff}=1.5$) in these compounds, their magnetic states are strongly affected below their phase

* Corresponding author.
E-mail address: skmisra@alcor.concordia.ca (S.K. Misra).

0304-8853/$ - see front matter © 2012 Elsevier B.V. All rights reserved.
http://dx.doi.org/10.1016/j.jmmm.2012.08.017

transitions, so that there occurs a competition between their ferro- and antiferro-magnetic states, which, in turn, affects their magnetoresistance.

2.1. Influence of Sm

Since the ionic radius of Sm (0.964 Å) is smaller than that of La (1.016 Å), the T_C decreases with increasing Sm concentration due to the magnetic interaction of Sm ions with (other) Sm and Mn ions, modifying the magnetic state of mixed La–Sm manganite. With increasing Sm content, the structure of the compound transforms from long-range ferromagnetic order for $La_{0.67}Sr_{0.33}MnO_3$ to spin-cluster glass state for the mixed La–Sm/Sr–Ba compound. The increase of Sm content also leads to distortion of Mn–O–Mn bonds and weakening of the double-exchange interaction in the Mn network, which governs ferromagnetic coupling, shifting the T_C to lower temperatures. In addition, there manifests extra magnetic coupling due to interactions among Sm ions, leading to a colossal magnetoresistance effect.

2.2. Influence of Ba

The ionic radius of Ba is larger than that of Sr; however the lattice constants are slightly smaller for $La_{0.67}Sr_{0.33}MnO_3$ with $a=5.5013$ Å and $b=13.36$ Å [9], as compared to those for $La_{0.67}Ba_{0.33}MnO_3$ with $a=5.5320$ Å and $b=13.5273$ Å [10]. Both $La_{0.67}Ba_{0.33}MnO_3$ and $La_{0.67}Sr_{0.33}MnO_3$ have rhombohedral structure with space group $R\bar{3}c$. Heavy Sm doping transforms its structure to orthorhombic with space group *Pnma*. It is noted that the structure of the mixed compound $(La_{0.33}Sm_{0.67})_{0.67}Sr_{0.33-x}Ba_xMnO_3$ is orthorhombic [1,3]. The lattice parameters increase with Ba doping as follows: $a=5.5056$ Å, $b=7.7801$ Å, and $c=5.5022$ Å for $(La_{0.33}Sm_{0.67})_{0.67}Ba_{0.33}MnO_3$, and $a=5.4722$ Å, $b=7.7063$ Å, and $c=5.4599$ Å for $(La_{0.33}Sm_{0.67})_{0.67}Sr_{0.33}MnO_3$, as reported by Asthana et al. [1]. Doping with Ba ions leads to inhomogeneous distribution of Mn^{4+} ions, which exhibit EPR signal in the manganites, and cause clustering, as evidenced in diluted Ba and Sr manganites [11,12]. Therefore, the regions enriched with Mn^{4+}–O–Mn^{4+} bonds in the sample tend to become dielectric, not participating in the electron-transfer process.

3. Synthesis

The samples were synthesized by the citrate sol–gel method based on citrate gel formation with ethylene glycol: Stoichiometric amounts of initial compounds, such as Sm_2O_3, La_2O_3, $SrCO_3$, $BaCO_3$, MnO_2, and Mn_2O_3, were dissolved in a minimal amount of nitric acid by continuous heating. Calculated amounts of ethylene glycol and citric acid were added after complete dissolution of the initial compounds. Thermal decomposition of the gel was carried out in a muffle furnace by slow heating from 100 °C to 800 °C. The samples so obtained were sintered at 1450 °C for 10 h. The completion of the reaction in the samples was verified by X-ray diffraction and chemical analysis. No second phase was detected in any samples by X-ray powder diffraction analysis.

4. EPR measurements

A Bruker ESP-300 EPR X-band spectrometer (9.46 GHz), equipped with a nitrogen-gas flow cryostat for temperature variation in the temperature range 110–450 K was used to investigate the samples. The spectra were recorded for both heating and cooling. Some hysteresis, less than 2 K, was found in the two sets of measurements, which is not significant. Thus, only the spectra recorded during cooling are considered here.

The EPR spectra for the various samples show paramagnetic EPR lines at high temperatures, which gradually change to ferromagnetic resonance (FMR) lines below the respective transition temperatures (T_C) for the samples with $x=0.01$, 0.03, and 0.06. No such transition is observed for the sample with $x=0.09$ over the temperature range of investigation; according to interpolation as discussed later it should be about 130 K, but it is masked by the line due to the Griffiths phase. The temperature variations of the EPR spectra for these samples are shown in Figs. 1,2,3 and 4, correspondingly.

The temperature variations of the EPR/FMR spectra of the samples with $x=0.01$, 0.03, and 0.06 near and below the respective phase-transition temperatures are shown in Fig. 1a (110–196 K), 2 (113–198 K), 3 (100–210 K), and for the sample with $x=0.09$ in Fig. 4 (110–230 K), respectively. These temperature ranges were chosen because only one Lorentzian line was observed at

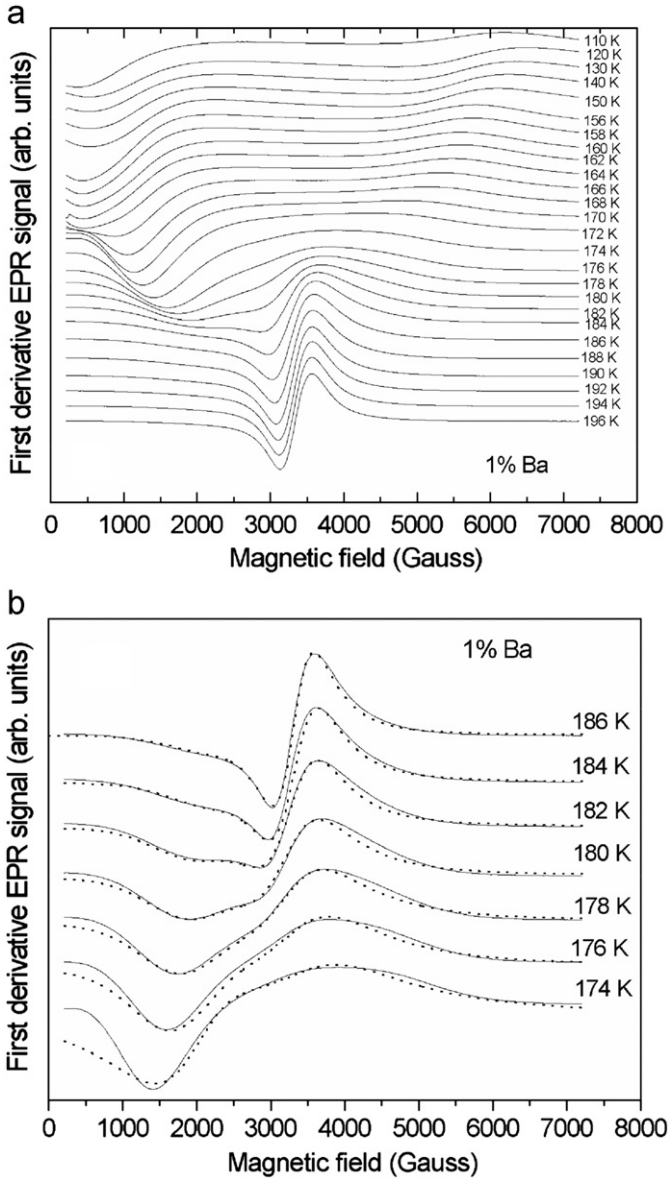

Fig. 1. A plot of EPR spectra of $(La_{1/3}Sm_{2/3})_{2/3}Ba_{0.01}Sr_{0.32}MnO_3$ sample ($x=0.01$) versus temperature. (a) EPR spectra at temperatures from 110 to 196 K. The transition temperature to ferromagnetic phase is $T_C=178\pm2$ K. and (b) EPR spectra in vicinity of phase transition (174–186 K) with its simulation as a sum of EPR and FMR signals, shown by dashed lines. The fitting parameters characterizing the FM and PM signals are listed in Table 1.

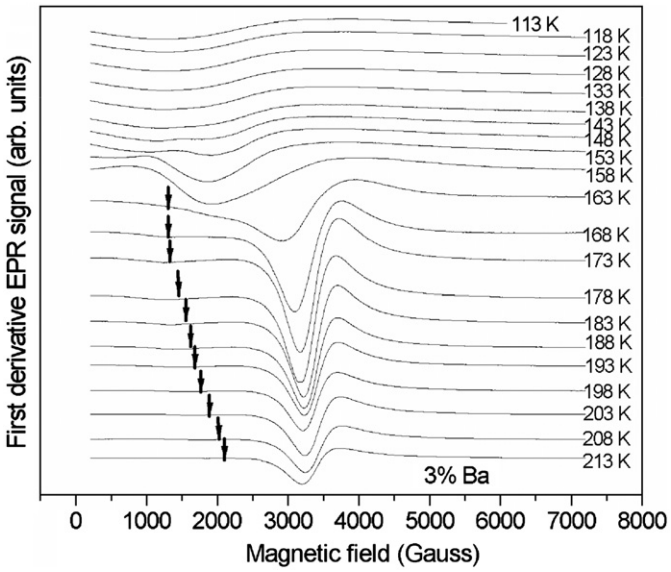

Fig. 2. Variation of the EPR spectra of $(La_{1/3}Sm_{2/3})_{2/3}Ba_xSr_{1-x}MnO_3$ ($x=0.03$) sample versus temperature from 100 to 213 K. The signal from Griffiths phase in the temperature region 178–218 K is clearly seen, and indicated by arrows. The transition temperature to ferromagnetic phase is $T_C=163\pm5$ K.

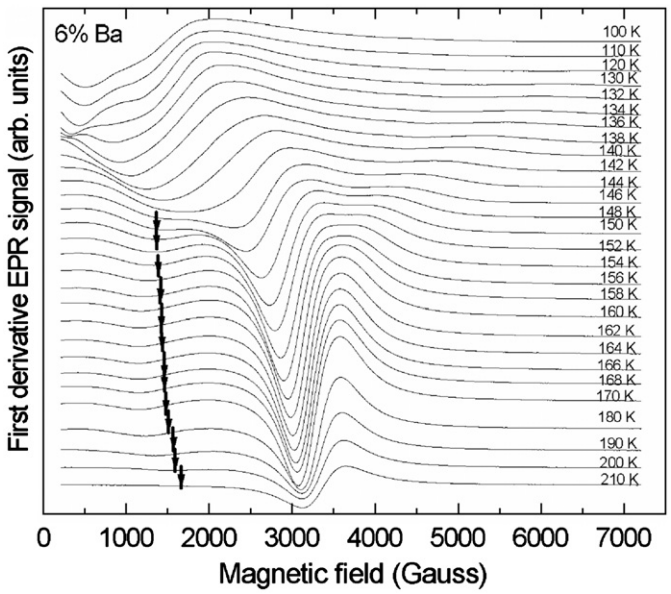

Fig. 3. Variation of the EPR spectra of $(La_{1/3}Sm_{2/3})_{2/3}Ba_xSr_{1-x}MnO_3$ ($x=0.06$) sample versus temperature from 100 to 210 K. The signal from Griffiths phase in the region 150–200 K is clearly seen, and indicated by arrows. The transition temperature to ferromagnetic phase is $T_C=142\pm2$ K.

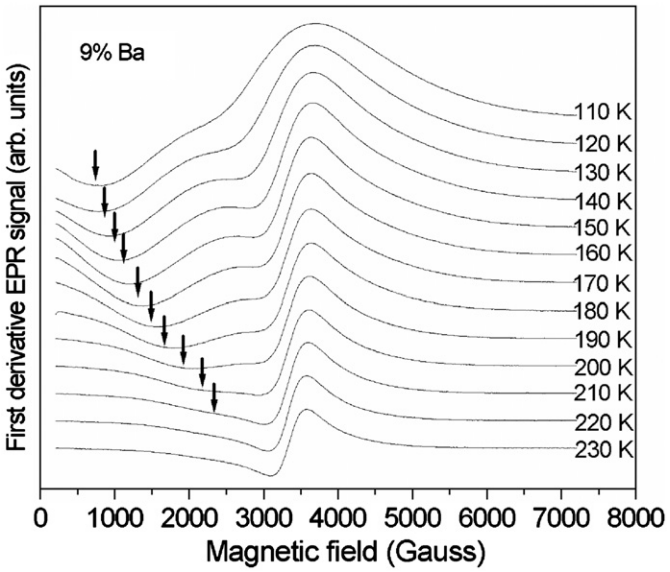

Fig. 4. Variation of the EPR spectra of $(La_{1/3}Sm_{2/3})_{2/3}Ba_xSr_{1-x}MnO_3$ sample with $x=0.09$ versus temperature from 110 to 210 K. The signals corresponding to Griffiths phase in the region 100–200 K are clearly seen, and indicated by arrows.

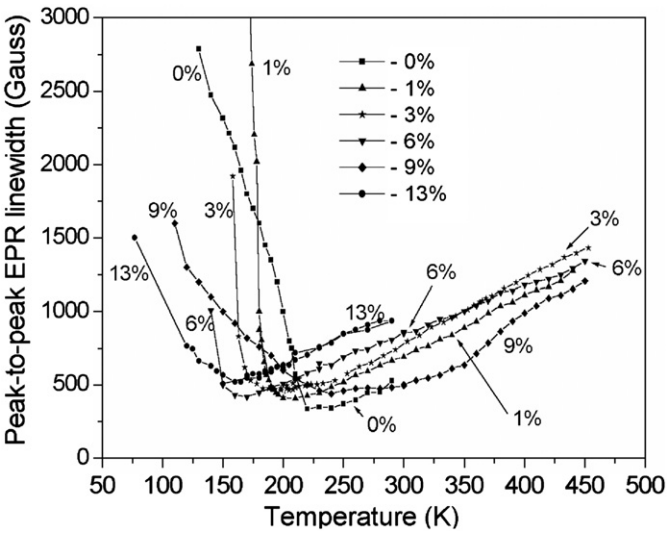

Fig. 5. Peak-to-peak EPR linewidths exhibited by the manganite samples versus temperature. Here the EPR linewidths for the samples with $x=0.0$, 0.01, 0.03, 0.06 and 0.09 are indicated by circles, squares, down triangles, up triangles, and stars, respectively. The EPR linewidths for the sample with $x=0$ and $x=0.13$, taken from [4], are also shown for comparison.

temperatures above 200 K, which is well above the phase-transition temperatures. The temperature dependences of the EPR linewidths for all four samples are shown in Fig. 5. The phase transition temperature, T_C, was determined from the temperature dependence of the EPR spectra, to be the temperature at which the transition to FMR lines occurs as the temperature is lowered. The dependence of T_C on Ba content is shown in Fig. 6.

4.1. Sample with $x=0.01$ (Fig. 1(a) and (b)).

Here the phase transition is clearly observed, similar to that for the sample $(La_{1/3}Sm_{2/3})_{2/3}Sr_{0.33}MnO_3$ [4], without any Ba doping. The phase-transition temperature is 178 ± 2 K. The shape of the EPR line over the temperature interval where the paramagnetic and ferromagnetic phases coexist was analyzed as follows. There exist two lines, one, corresponding to the paramagnetic phase with $g=2.0$, and the second, corresponding to the ferromagnetic phase, with g value increasing with decreasing temperature below the phase-transition temperature. The overall experimental EPR line over this temperature can be easily simulated to be a sum of these two lines as shown in Fig. 1(b); the parameters of these two lines (g-values, lineshape, linewidth and relative intensity) are given in Table 1. The line corresponding to the paramagnetic phase is assumed to be Lorentzian, caused by the motional effect due to the exchange interaction between electronic spins [13], whereas the line corresponding to the ferromagnetic state is assumed to be Gaussian in shape due to distribution of the directions of the moments of the various ferromagnetic

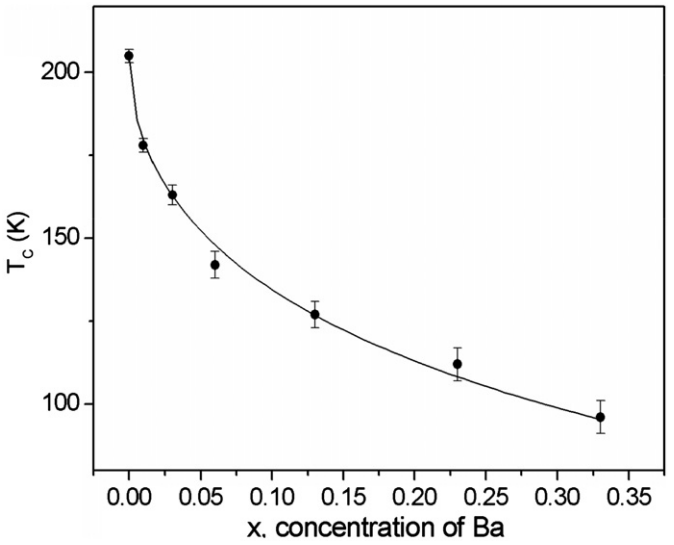

Fig. 6. Phase-transition temperature (T_C) versus Ba content; the continuous line represents fitting with the use of Eq. (3).

Table 1
Parameters of FM (Gaussian) and PM (Lorentzian) signals, used for the simulation of EPR line.

Temperature (K)	Linewidth (G)		g-value		Relative intensity	
	PM	FM	PM	FM	PM	FM
174	2000	1300	2.10	3.35	0.34	0.66
176	1400	1200	2.10	3.1	0.55	0.45
178	1200	1200	2.11	3.1	0.67	0.33
180	1000	1200	2.10	2.9	0.8	0.2
182	810	1200	2.07	2.8	0.9	0.1
184	670	1200	2.04	2.7	0.98	0.02
186	560	1100	2.04	2.7	0.99	0.01

clusters in the sample. The transition temperature to ferromagnetic phase is $T_C=178\pm2$ K.

4.2. Sample with $x=0.03$ (Fig. 2)

The EPR line in the paramagnetic phase appears to be asymmetrical, due to overlap of the EPR line due to Griffiths phase. The phase transition from the paramagnetic to ferromagnetic phase occurs in a smooth, gradual manner. The EPR signal in this sample can be expressed as a sum of EPR and FMR signals in the temperature range 158–168 K below the phase-transition temperature similar to that in the samples with $x=0$ [4] and $x=0.01$. The transition temperature to ferromagnetic phase is $T_C=163\pm5$ K. Along with the intense paramagnetic lines, there were observed EPR lines with rather low intensities at lower magnetic fields, similar to those observed in the samples with $x=0.13$, and 0.23 [4], which correspond to Griffiths phase [14–16]. The linewidth of these lines changes from 150 G at 218 K to 450 G at 168 K.

4.3. Sample with $x=0.06$ (Fig. 3)

There are observed similar lines here to those observed in samples with $x=0.01$ and 0.03. The shape of the EPR lines is slightly asymmetrical, like that of a Dysonian line [17]. The FMR line in addition to that due to Griffiths phase, was also observed here, as shown in Fig. 3. Its linewidth increases from 300 G at 210 K to 850 G at 160 K. The transition temperature to ferromagnetic phase is $T_C=142\pm2$ K.

4.4. Sample with $x=0.09$ (Fig. 4)

Intense lines, corresponding to Griffiths phase similar to those observed in the samples with $x=0.03$ and 0.06, were observed along with the paramagnetic lines at lower fields over a wide temperature range, up to room temperature. This behavior is similar to that, observed for EPR signal in the paramagnetic phase in $Eu_{0.6}La_{0.4-x}Sr_xMnO_3$ [18] for samples with x from $x=0.13$ to $x=0.2$. Paramagnetic and ferromagnetic phases should co-exist in this sample To this end, it is argued in [18] that possibly the magnetic Eu^{3+} ions favor a stabilization of ferromagnetic state in $Eu_{0.6}La_{0.4-x}Sr_xMnO_3$, and thus increase the intensity of EPR signals due to Griffiths phase signals over a wide temperature region. The transition temperature to ferromagnetic phase is difficult to determine as the ferromagnetic lines are presumably masked by the predominant lines due to Griffiths phase, but by extrapolation it appears to be about 125 K (see Fig. 6).

The T_C values for the samples with $x=0.13$, 0.23, and 0.33 were determined from the temperature dependence of magnetic susceptibility [1]. These values are shown in Fig. 6.

4.5. Griffiths phase

As mentioned above, there were observed another set of EPR lines at low magnetic fields, attributed to nanosized ferromagnetic clusters (ferrons) [14–16]. These additional lines are clearly seen in the spectra shown in Fig. 2b (sample with $x=0.03$), Fig. 3 (sample with $x=0.06$), and Fig. 4 (sample with $x=0.09$). These ferron structures occur due to disorder caused by displacements of Sr^{2+} ions by Ba^{2+} ions. This leads to creation of holes located at the positions of the Mn, or oxygen, ions, which migrate to the Mn^{3+} sites, causing polarization of the direction of spins, leading to the formation of ferromagnetically ordered nanostructures.

The nature of the so-called Griffiths phase can be interpreted in terms of a Griffiths singularity arising due to the presence of quenched disorder (QD) in the orthorhombic phase of these manganites [14–16]. Griffiths phase is characterized by a random distribution of dilute magnetic entities subjected to slow spin dynamics [19]. In manganites, QD is due to the random distribution of the ions in the pervoskite A-site in $Ln_{1-x}A_xMnO_3$ ($Ln=La^{3+}$, Sm^{3+}, etc. and $A=Sr^{2+}$, Ba^{2+}, etc.). The magnitude of the QD is related to the difference in the ionic radii of the cations Ln and A. The disorder within Ln and A sublattice can increase this effect. Thus, the formation of Griffiths phase in $(La_{1/3}Sm_{2/3})_{2/3}Sr_{0.33-x}Ba_xMnO_3$ system is due to Sr/Ba disorder, which leads in its turn to Mn^{3+}/Mn^{4+} disorder. Therefore no Griffiths phase was observed in the samples with $x=0$ (no Ba) and $x=0.33$ (no Sr), which do not have simultaneous presence of Ba and Sr ions [4].

5. EPR linewidth

5.1. Temperature dependence of the EPR linewidth in the paramagnetic phase

The variable-range-hopping (VRH) model has been used here to explain the temperature dependence of the EPR linewidth in the paramagnetic temperature range of lightly doped samples of the manganites $(La_{033}Sm_{0.67})_{0.67}Sr_{0.33-x}Ba_xMnO_3$ ($x=0.01$, 0.03, 0.06, and 0.09) based on their conductivity properties [3] as supported by experimental data. These compounds become disordered due to the introduction of Ba atoms to partially replace Sr atoms. With the increase of disorder in the system, the conductivity mechanism changes from small polaron hopping to variable range hopping [20].

Recently, a new approach has been proposed by Vekilov and Malkovskii [21] to explain the conductivity in the manganites, based on the VRH model. In this approach VRH in manganites is described by the model of metallic-like droplets embedded in a dielectric matrix. The VRH mechanism becomes effective due to the two-phase state of the system, comprising metallic (ferromagnetic) and dielectric (paramagnetic) phases. When the density of the metallic droplets is less than the percolation limit, the sample is in the insulating (paramagnetic) state with VRH conductivity defined by inter-granular tunneling and electrostatic barriers. As the temperature increases the VRH regime is transformed into the hopping regime of small radius polarons. The VRH regime in manganites is not due to structural disorder; rather it is due to the size of metallic droplets, which define the magnetic nature of the sample. If it is sufficiently large, it results in the ferromagnetic state to produce an FMR signal. In the present data, it occurred in the samples with $x=0.01$ and 0.03 near the respective phase-transition temperatures. The metallic droplets with nano-size in the paramagnetic phase can be considered as ferrons, which give rise to Griffiths phase. The density of such ferrons, distributed over the whole sample, determines the intensity of the EPR signal due to Griffiths phase. In the present considerations, the VRH model was used within the framework of Mott's model [22], which has been used to explain the experimental data on manganite conductivity, and allows one to compare the data obtained from conductivity with those of EPR linewidth.

In previous investigations of EPR spectra of $(La_{033}Sm_{0.67})_{0.67}Sr_{0.33-x}Ba_xMnO_3$, ($x=0.0$, 0.13, 0.23, and 0.33), evidence of exchange narrowing of EPR lines near T_{min} was found, where the linewidth exhibits the minimum. The well-known small-polaron hopping model for the interpretation of EPR linewidth in the paramagnetic region [23] was used to explain the linewidth behavior. In this model, influence of small-polaron hopping conductivity in the paramagnetic state in highly doped manganite samples $(La_{033}Sm_{0.67})_{0.67}Sr_{0.33-x}Ba_xMnO_3$ ($x=0.0$, 0.13, 0.23, and 0.33), [4], accompanied by flip-flop of spins, during the electron transfer from Mn^{3+} to Mn^{4+} state, is considered to lead to broadening of EPR linewidth.

As stated above, increasing disorder in the distribution of Mn^{4+} and Mn^{3+} ions due to doping with Ba ions requires the application of variable-range-hopping (VRH) model for the charge-transfer process in manganites. Accordingly, the temperature dependence of conductivity can be expressed as [22]

$$\sigma = \sigma_0 \exp\left(-(T_0/T)^{1/4}\right) \quad (1)$$

where T_0 is the characteristic temperature; its value for manganites is around 10^6 K.

Assuming that the EPR linewidth is proportional to the conductivity in $(La_{1/3}Sm_{2/3})_{2/3}Sr_{1/3-x}Ba_xMnO_3$, whose behavior is governed by the VRH model, the EPR linewidth can be similarly expressed as

$$\Delta B_{pp}(T) = \Delta B_{pp,min} + C\exp\left(-(T_0/T)^{1/4}\right) \quad (2)$$

In Eq. (2), $T_0=18\alpha^3/kN(E_p)$, E_p is the electron density; $L=1/\alpha$ is the localization length; it is on the order of distance between adjacent Mn ions. Its average value is 2.2 nm. As estimated for $La_{0.7}Sr_{0.3}MnO_3$, $kT_0=220$ eV ($T_0=2.55\times10^6$ K) [24,25]. T_0 was estimated from Eq. (4), for $(La_{033}Sm_{0.67})_{0.67}Sr_{0.33}MnO_3$, to be 1.7×10^6 K, in reasonable agreement with those for $La_{0.7}Sr_{0.3}MnO_3$ ($T_0=2.55\times10^6$ K), $La_{0.35}Pr_{0.15}Ca_{0.16}Sr_{0.34}MnO_3$ ($T_0=1.5\times10^6$ K), and $La_{0.31}Sm_{0.19}Sr_{0.5}MnO_3$ ($T_0=2.8\times10^6$ K) manganites, characterized by disorder in rare-earth and alkaline-earth ions. VRH conductivity mechanism clearly applies for explanation of charge transfer in all these compounds [26]. It is noted that the VRH model was also used to explain the electrical properties of $(La_{0.4}Sm_{0.6})_{0.67}Sr_{0.33}MnO_3$, which is quite similar to $(La_{033}Sm_{0.67})_{0.67}Sr_{0.33}MnO_3$, in the paramagnetic region [3].

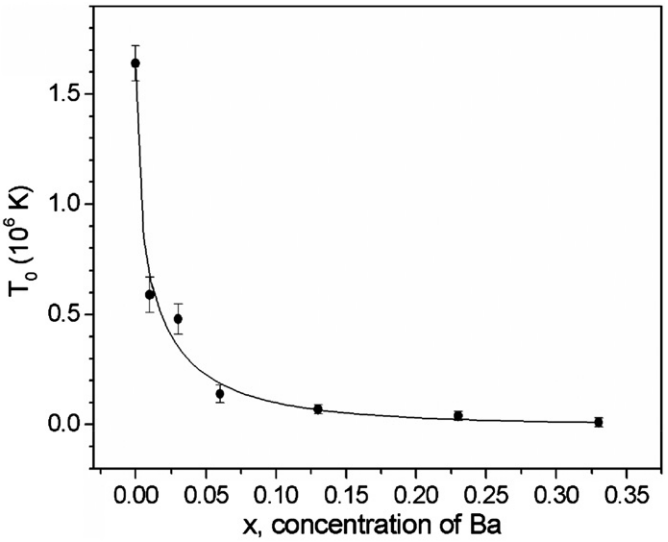

Fig. 7. Plot of the parameter of the variable-range-hopping model, T_0, versus Ba content, as estimated by the use of Eq. (2). The continuous line represents fitting with the use of Eq. (4).

Eq. (2) was used to evaluate the VRH parameter T_0. This parameter was estimated for the samples $(La_{1/3}Sm_{2/3})_{2/3}Sr_{1/3-x}Ba_xMnO_3$ ($x=0.0$, 0.01, 0.03, 0.06, and 0.13, 0.23, 0.33) from the dependence of EPR linewidth on temperature in the paramagnetic phase of these samples. The required EPR data for $x=0.0$, 0.13, 0.23, and 0.33, not investigated here, are taken from [4], (The EPR data for $x=0.09$ are not included due to the predominant EPR lines due to Griffiths phase for this sample as discussed above.) The various values are plotted in Fig. 7, which reveals that T_0 decreases with increasing Ba content. This decrease is found to be quite sharp for the Ba-content $x=0.0$–0.1.

5.2. Behavior of transition temperature (T_C)

The transition temperatures to the ferromagnetic state of these samples gradually decreased from 178 K for the sample with $x=0.01$ to 163 K for the sample with $x=0.03$, and to 142 K for the sample with $x=0.06$. It is noted that even 1% Ba doping shifts the ferromagnetic phase transition by more than 27 K down from its value in the sample without Ba doping, $(La_{0.33}Sm_{0.67})_{0.67}Sr_{0.33}MnO_3$ ($T_C=205$ K). This is due to significant structural changes effected by even very small amount of Ba^{2+} ions substituting for Sr^{2+} ions in the samples with $x=0.01$, 0.03, 0.06. and 0.09.

5.3. Dependence of T_C and T_0 on Ba content (x)

The VRH parameter T_0 changes with temperature in the same way as does T_C. It is possible to fit both dependences, T_C and T_0 versus Ba content (x), with the following empirical expressions:

$$T_C(x) = T_C(0)\exp\left(-C_1x^{1/2}\right) \quad (3)$$

$$T_0(x) = T_0(0)\exp\left(-C_2x^{1/2}\right) \quad (4)$$

In Eqs. (3) and (4), best fitting provides the values of the parameters: $C_1=1.33\pm0.03$, $C_2=0.89\pm0.06$, $T_C(0)=205$ K, and $T_0(0)=1.64\times10^6$ K. Using these, the dependences of T_C and T_0 on x are shown in Figs. 6 and 7, respectively.

These dependences can be explained as follows. Both charge transfer and magnetic-ordering processes depend strongly on

Mn–O–Mn bonding in the structure of manganites. If the distance r between Mn and O ions changes, the value of the overlap integral between Mn and O electron density changes as exp $(-Cr)$, where, C is a constant. This affects the values of charge transfer and magnetic-ordering parameters. Finally, expressions (3) and (4) reveal that both T_C and T_0 depend on Ba concentration in the same exponential manner.

6. Concluding remarks

The salient features of the EPR study on the lightly Ba-doped manganite samples of $(La_{1/3}Sm_{2/3})_{2/3}Sr_xBa_{0.33-x}MnO_3$ ($x=0.01$, 0.03, 0.06, 0.09) presented in this paper are as follows:

(i) The substitution of Sr^{2+} ions by Ba^{2+} ions in these lightly doped samples has a profound effect on T_C, the ferromagnetic phase-transition temperature. T_C decreases by a rather large amount, from 205 K for the sample with $x=0$ to 178 K for $x=0.01$, by the change in x by only a small amount of 0.01. On the other hand, in heavily doped samples, when Ba content changes from $x=0.13$ to $x=0.33$, e.g., by 0.2, T_C changes only by a small amount of 31 K, from 127 to 96 K.

(ii) The application of variable-range-hopping-mechanism correctly explains the dependence of the EPR linewidth on temperature in the paramagnetic region, which is consistent with the conductivity data.

(iii) Griffiths phase, characterized by the coexistence of ferron nanostructures and paramagnetic bulk state, was clearly observed in the sample with $x=0.03$, 0.06, and 0.09.

Acknowledgments

S.K.M. is grateful to the Natural Sciences and Engineering Research Council of Canada for partial financial support. S.I.A. is grateful to the Ministry of Education of Russian Federation. The authors thank Prof. B.I. Kochelaev for helpful discussion and his interest in this work.

References

[1] S. Asthana, A.K. Nigam, S.K. Malik, D. Bahadur, Lattice effect on the magnetic and magneto-transport properties of $(La_{1/3}Sm_{2/3})_{2/3}Ba_{0.33-x}Sr_xMnO_3$ ($x=0.0$, 0.1, 0.2 and 0.33) compounds, Journal of Alloys and Compounds 450 (1–2) (2008) 136–141.

[2] S. Astana, D. Bahadur, A.K. Nigam, S.K. Malik, Electronic phase separation in $(La_{1/3}\ Sm_{1/3}\ )A_{1/3}MnO_3$ (A=Ca, Sr, and Ba) compounds, Journal of Applied Physics 97 (2005) 10H711.

[3] Guo Huanyin, Liu Ning, Yan Guoqing, Tong Wei, Transport property of $La_{0.67-x}Sm_x\ Sr_{0.33}\ MnO_3$, at heavy samarium doping ($0.40 \le x \le 0.60$), Journal of Rare Earths 16 (3) (2006) 206–213.

[4] S.K. Misra, S.I. Andronenko, S. Asthana, D. Bahadur, A variable temperature EPR study of the manganites $(La_{1/3}Sm_{2/3})_{2/3}Sr_xBa_{0.33-x}MnO_3$ ($x=0.0$, 0.1, 0.2, and 0.33): small polaron hopping conductivity and Griffiths phase, Journal of Magnetism and Magnetic Materials 322 (19) (2010) 2902–2907.

[5] Q. Huang, A. Santoro, J.W. Lynn, R.W. Erwin, J.A. Borchers, J.L. Peng, R.L. Greene, Structure and magnetic order in undoped and doped manganites, Physical Review B 55 (22) (1997) 14987–14999.

[6] G.N. Jonker, J.H. van Santen, Ferromagnetic compounds of manganese with perovskite structure, Physica 16 (3) (1950) 337–349.

[7] R. von Helmolt, J. Wecker, B. Holzapfel, L. Schultz, K. Samwer, Giant negative magnetoresistance in perovskitelike $La_{1/3}Ba_{2/3}MnO_3$ ferromagnetic films, Physical Review Letters 71 (14) (1993) 2331–2333.

[8] C. Autret, M. Gervais, F. Gervais, N. Raimboux, P. Simon, Signature of ferromagnetism, antiferromagnetism, charge ordering and phase separation by electron paramagnetic resonance study in rare earth manganites, $Ln_{1-x}A_xMnO_3$ (Ln=rare earth, A=Ca,Sr), Solid State Sciences 6 (8) (2004) 815–824.

[9] M.T. Causa, M. Tovar, A. Caneiro, F. Prado, G. Ibañez, C.A. Ramos, A. Butera, B. Alascio, X. Obradors, S. Piñol, F. Rivadulla, C. Vázquez-Vázquez, M.A. López-Quintela, J. Rivas, Y. Tokura, S.B. Oseroff, High-temperature spin dynamic in CMR manganites: ESR and magnetization, Physical Review B 58 (6) (1998) 3233–3239.

[10] Y.B. Zhang, S. Li, C.Q. Sun, W. Gao, Possible origin of magnetic transition ordering in $La_{1/3}A_{2/3}MnO_3$ oxides, Materials Science and Engineering B 98 (1) (2003) 54–59.

[11] S.I. Andronenko, R.R Andronenko, O.A. Zagrebel'nyi, N.V. Chezhina, EPR study of compounds in the $LaAlO_3$—$Ln_{0.67}Sr_{0.33}MnO_3$ system, Glass Physics and Chemistry 35 (6) (2009) 652–659.

[12] S.I. Andronenko, R.R. Andronenko, O.A. Zagrebel'nyi, EPR study of $La_{1-0.33y}Ba_{0.33y}Mn_yAl_{1-y}O_3$ ($y=0.02$, 0.04, 0.10) solid solutions, Glass Physics and Chemistry 36 (5) (2010) 617–622.

[13] S.K. Misra, in: C. Poole Jr., H.A. Farach (Eds.), Handbook of Electron Spin Resonance, Ed,Springer, N.Y, 1999.

[14] R.M. Eremina, J.V. Yatsyk, Ya.M. Mukovskii, H.-A. Krug von Nidda, A. Loidl, Determination of the region of existence of ferromagnetic nanostructures in the paraphrase of $La_{1-x}Ba_xMnO_3$ by the EPR method, JETP Letters 85 (1) (2007) 51–54.

[15] J. Deisenhofer, D. Braak, H.-A. Krug von Nidda, J. Hemberger, R.M. Eremina, V.A. Ivanshin, A.M. Balbashov, G. Jug, A. Loidl, T. Kimura, Y. Tokura, Observation of a Griffiths phase in paramagnetic $La_{1-x}Sr_xMnO_3$, Physical Review Letters 95 (25) (2005) 257202.

[16] O.A. Yassin, M.I. Mohamed, S.N. Bhatia, Effects of quenched disorder on Griffiths phase and EPR line width in $La_{0.67-2x}Nd_{2x}Ca_{0.33-x}Sr_xMnO_3$ manganites, Physica Status Solidi (b) 245 (4) (2008) 745–749.

[17] F.J. Dyson, Electron spin resonance absorption in metals. II. Theory of electron diffusion and the skin effects, Physical Review 98 (2) (1955) 349–359.

[18] R.M. Eremina, I.I. Fazlizhanov, I.V. Yatsyk, K.R. Sharipov, A.V. Pyataev, H.-A. Krug von Nidda, N. Pascher, A. Loidl, K.V. Glazyrin, Ya.M. Mukovskii, Phase separation in paramagnetic $Eu_{0.6}La_{0.4-x}Sr_xMnO_3$, Physical Review B 84 (6) (2011) 064410.

[19] A.J. Bray, Nature of the Griffiths phase, Physical Review Letters 59 (5) (1987) 586–589.

[20] C. Rettori, D. Rao, J. Singley, D. Kidwell, S.B. Oserroff, M.T. Causa, S-W. Cheong, S. Schultz, Temperature dependence of the ESR linewidth in paramagnetic phase ($T > T_C$) of $R_{1-x}B_xMnO_{3+\delta}$ (R=La, Pr; B=Ca, Sr), Physical Review B 55 (5) (1997) 3083–3086.

[21] Yu.Kh. Vekilov, Ya.M. Mukovskii, Variable range hopping conductivity in manganites, Solid State Communications 152 (13) (2012) 1139–1141.

[22] N.F. Mott, Metal–insulator transitions, Taylor and Francis, London, 1990 286 p.

[23] A. Shengelaya, Guo-meng Zhao, H. Keller, K.A. Muller, B.I. Kochelaev, EPR in $La_{1-x}Ca_xMnO_3$: relaxation and bottleneck, Physical Review B 61 (9) (2000) 5888–5890.

[24] J.M.D. Coey, M. Viret, L. Ranno, K. Ounadjela, Electron localization in mixed-valence manganites, Physical Review Letters 75 (21) (1995) 3910–3913.

[25] M. Viret, L. Ranno, J.M.D. Coey, Magnetic localization in mixed-valence manganites, Physical Review B 55 (13) (1997) 8067–8070.

[26] Irfan Mansuri, Dinesh Varshney, N. Kaurav, C.L. Lu, Y.K. Kuo, Effects of A-site disorder on magnetic, electrical and thermal properties of $La_{0.5-x}Ln_x$-$Ca_{0.5-y}Sr_yMnO_3$ manganites, Journal of Magnetism and Magnetic Materials 323 (3–4) (2011) 316–323.